JOURNAL OF MATERIALS SCIENCE 15 (1980) 859–870

The ageing characteristics of an Fe-19 wt% Ni-9 wt% Co-5 wt% W alloy

C. SERVANT, P. LACOMBE
Laboratoire de Métallurgie Physique, associé au CNRS no. 177, Université de Paris-Sud, Centre d'Orsay, 91405 Orsay Cedex, France

M. GRIVEAU
Laboratoire de Métallurgie de l'Ecole Nationale Supérieure des Arts et Métiers, 151 bd de l'Hôpital, 75640 Paris Cedex 13, France

In the present paper, we compare the behaviour during ageing in the temperature range 380 to 530° C of the two martensitic alloys Fe–18.65 Ni–8.99 Co–4.87 Mo and Fe–18.65 Ni–8.99 Co–4.87 W (wt %). The kinetics of precipitation were followed by measurements of hardness, by resistometric measurements and electron microscopy. In the case of the alloy with Mo, Mo at first concentrates in local clusters, then an ω phase is formed, and above 450° C, finally a Ni_3Mo or Laves phase $(Fe, Ni, Co)_2Mo$ is formed. In the case of the alloy with W, ω phase formation was not observed but an intermetallic precipitate isomorphous with Ni_3Mo, $(Fe, Ni, Co)_3W = A_3W$ was found. The precipitates are rod-shaped, of several nm in length. The preferred direction of growth of these precipitates is $\langle 1\,1\,1\rangle$ of the martensitic matrix and the orientation relationship with the martensitic matrix is $(0\,1\,1)_M \parallel (0\,1\,0)_{A_3W}$ and $[1\,\bar{1}\,1]_M \parallel [1\,0\,0]_{A_3W}$, identical to that found for the Ni_3Mo precipitate in the (Fe, Ni, Co, Mo, Ti) industrial maraging steel.

1. Introduction

Among the alloys with a martensitic structure in which an age-hardening phenomenon occurs (called maraging), the most simple are the ternary alloys Fe–Ni–X and the quaternary alloys Fe–Ni–Co–X. In order to obtain a lath martensitic structure, the percentage of Ni ranges between 12 and 20 wt %, that of Co between 8 and 10 wt %, and X is an element which is responsible for the strengthening phenomenon, e.g. Mo, Ti and W. Studies concerning the hardening phenomenon have been largely confined to the alloys containing Mo and Ti [1–30]; information on W-containing alloys is lacking although this element has physical and chemical properties very similar to that of molybdenum [23, 31].

The present investigation was made to compare the structural transformations in the alloys Fe–18.65 Ni–8.99 Co–4.87 W (wt %) with those in an alloy of the same Fe, Ni and Co contents with Mo instead of W. The results on the alloy Fe–18.65 Ni–8.99 Co–4.87 Mo (wt %) have been previously published [30].

2. Experimental procedure

2.1. Preparation and structure of the alloy

The (Fe, Ni, Co, W) alloy was prepared from the mixtures of high purity powders* [23] by solid state sintering processing. The green pellets were compressed under a pressure of 5 tons cm^{-2} and then sintered at 1400° C for 4 h†. The samples were rolled to the required thickness using several intermediate anneals at 1400° C and cooled to room temperature at an average rate of 600° Ch^{-1}.

* The Fe and Ni powders are of ex-carbonyl origin and the Co and W powders are obtained by the reduction of CoO_3 and WO_3 by H_2

† The anisothermal and isothermal anneals for preparation and homogenization of the alloys, were carried out under purified hydrogen.

0022–2461/80/040859–12$03.20/0

Within the scale of the microprobe analysis, the alloy is homogeneous and its structure consists of lath martensite.

2.2. Experimental methods

The dilatometric analysis was carried out with a DHT 60 type differential dilatometer. In this apparatus, the length of the sample is continuously compared with a standard alumina sample. The magnification coefficient was equal to 1530 and the dimensions of the samples were as follows: 15 mm x 3 mm x 1.5 mm [23].

The resistivity measurements were made at the ageing temperature using a potentiometric apparatus [23], with samples of 180 mm x 5 mm x 0.1 mm; these samples were wound into a spiral 50 mm in length, this value being smaller than the length of the zone of homogeneous temperature in the furnace.

The hardness measurements were performed at room temperature under a load of 20 kg, on samples 10 mm x 4 mm x 3 mm. These samples were previously aged in a DITIRC dilatometer [28]. With this apparatus, the time to reach the temperature of 450° C is between 1 and 2 min. For each hardness value plotted, ten measurements were taken.

The lattice parameter measurements were carried out using the back reflection Debye–Scherrer method with a flat film, using as a standard a thin layer of copper powder coated onto the samples.

The electron microscopy examinations were carried out with a JEOL 100 C at a tension of 100 kV. The thin foils were obtained by anodic dissolution at 20 volts in a bath containing: 100 g chromic anhydride; 540 cm^3 acetic acid (density = 1.33); and 30 cm^3 distilled water.

3. Results and discussion

3.1. Comparison of the behaviour of the Fe, Ni, Co, W and Fe, Ni, Co, Mo alloys during anisothermal heating

At 20° C, the structure of these two alloys is single-phased and consists of lath martensite.

During the course of a simple cycle consisting of heating at the average rate of 300° C h^{-1} between 20 and 950° C, and cooling at the average rate of 450° C h^{-1}, the behaviour of these two

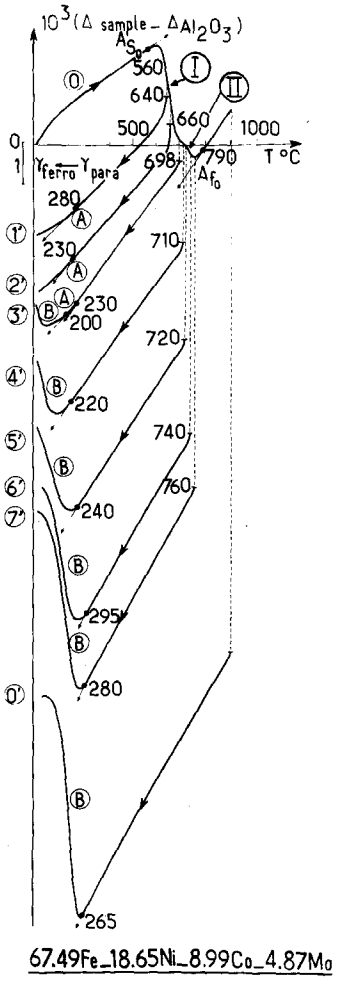

Figure 1 Dilation curves (under hydrogen atmosphere) for the Fe–Ni–Co–Mo alloy during cooling (450° C h^{-1}) from different temperatures in the austenitic transformation range.

alloys is similar. From the dilatometric curves of heating shown in Figs. 1 and 2, it appears that the martensite → austenite transformation occurs in two distinct stages designated by (I) and (II), which both represent contraction. The curves obtained by cooling from the temperatures between the two points $A^*_{s_0}$ and $A^*_{f_0}$ give:

(i) either no M_s point (curves 1′, 2′, Figs. 1 and 2) and the austenite formed between A_{s_0} and 640 or 698° C (Fig. 1) was stable down to room temperature;

(ii) or the Curie point of the austenite corresponding to the magnetic transformation $\gamma_{paramagnetic} \rightarrow \gamma_{ferromagnetic}$, marked (A) in Fig. 1,

* The A_{s_0} and M_{s_0} points are respectively the temperatures of the beginning of the martensite ⇄ austenite transformation of the alloy previously homogenized at 1400° C in the γ field. The subscript 0 is used to avoid confusion with the different A_s and M_s points obtained during those thermal cycles which were interrupted at some temperature between the A_{s_0} and A_{f_0} points.

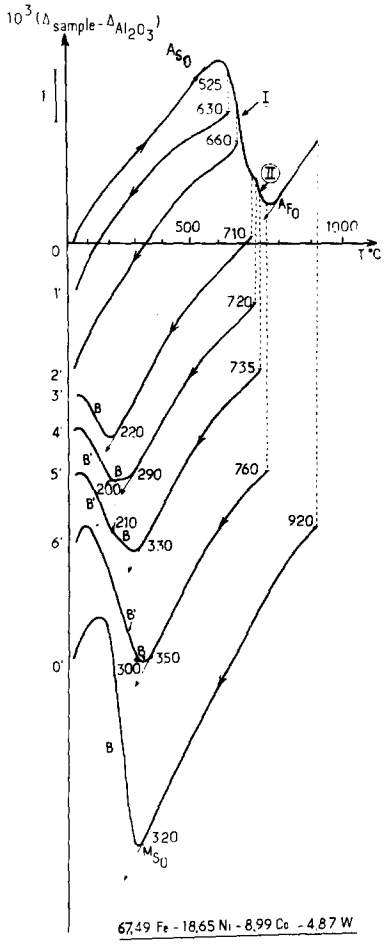

Figure 2 Dilation curves (under hydrogen atmosphere) for the Fe–Ni–Co–W alloy during cooling (450° C h^{-1}) from different temperatures in the austenitic transformation range.

curve 3′, and the M_s point of the structural transformation $\gamma_{ferromagnetic} \rightarrow M_{ferromagnetic}$, marked (B), in Fig. 1, curve 3′.

(iii) or two successive M_s points corresponding to the transformation $\gamma \rightarrow M$ in two successive stages designated by (B) and (B′). See Fig. 2, curves 4′, 5′, 6′.

These results show that during the course of heating between 20° C and A_{s_0}, the martensite with concentration of (Ni + X) = C_0, where X = Mo or W, ages progressively and decomposes into zones which are respectively enriched in (Ni + X), designated as M_R, and depleted in (Ni + X), designated as M_P. The M_R martensite transforms into austenite by a predominantly diffusional mechanism during the step I, while the M_P martensite transforms during the step II according to the following process:

$$M_R \rightarrow M_{RP} + \gamma_{RR}$$

$$M_P \rightarrow M_{PP} + \gamma_{PR}$$

So during the course of cooling from temperatures between the A_{s_0} and the A_{f_0} points the γ_{RR} and γ_{PR} austenites may or may not transform into two distinct martensites at the M_{s_P} and M_{s_R} points, depending upon the composition of these two austenites γ_{PR} and γ_{RR}.

The formation of compositional heterogeneities during heating to the A_{s_0} point is well revealed during isothermal ageing tests.

3.2. The formation of precipitates during isothermal ageing

From the resistivity and hardness measurements, three successive stages could be observed during the isothermal ageing, the nature of which is known from earlier work for the alloy with Mo.

3.2.1. In the case of the alloy with Mo addition

At temperatures lower than 450° C, the first stage is known to correspond to some clusters of 0.5 to 0.6 nm diameter, based on molybdenum [26, 27]. During the second stage zones enriched in molybdenum with quasi-spherical form of several nm in diameter are formed and increased in volume [21–23, 24]. Reversed austenite is formed during stage III.

The first two phenomena give rise to two successive decreases of resistivity, while the third phenomenon produces an increase in the resistivity. The atomic composition of the zones formed, ranges from A_8B to A_2B where A represents Fe, Ni and Co, and B represents Mo [21–24]. The parameters of the superstructure of type A_8B to A_7B_2 are,

$$a = a[1\,1\,\bar{2}]_M = a_M\sqrt{6} = 0.704\,\text{nm}$$

$$c = \frac{a}{2}[1\,1\,1]_M = a_M\frac{\sqrt{3}}{2} = 0.248\,\text{nm}$$

while the parameters of the superstructure A_2B are respectively equal to [24]

$$a = a_M\sqrt{2} = 0.3818\,\text{nm}$$

$$c = a_M\frac{\sqrt{3}}{2} = 0.2338\,\text{nm}$$

This structure of type A_2B has previously been identified as that of ω phase [24]. For temperatures higher than 450° C, the ω phase is no longer

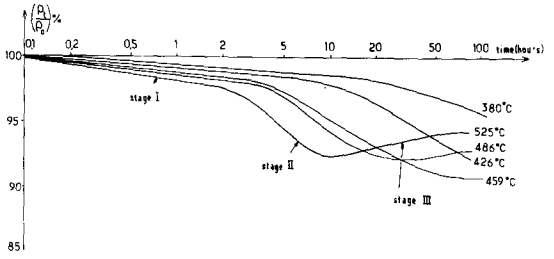

Figure 3 Isothermal resistivity curves (under hydrogen atmosphere) for the Fe–Ni–Co–W alloy.

formed, but intermetallic precipitates of the type Ni_3Mo or Laves phase of type $(Fe, Ni, Co)_2Mo$ is formed.

3.2.2. *In the case of the alloy with W addition*

The resistivity measurements (Fig. 3) showed that, unlike case 1, there are no differences in behaviour between the temperatures above or below 450° C. Two successive decreases of the resistivity corresponding to precipitation are observed, followed by an increase of the resistivity corresponding to the formation of the reversed austenite. The hardness tests also revealed three successive stages (Fig. 4):

Stage I which occurs during the early stages of the ageing (i.e. up to fifteen minutes) exhibits an increase in the hardness followed either by a plateau or by a slight decrease at the higher temperature studied (i.e. 505° C). The plateau generally appears after a few minutes of ageing. Whatever the ageing temperature within the range 400 to 500° C, there is an increase in hardness (between the time $t = 0$ and the time t corresponding to the beginning of the plateau) equal to 40 HV; this increase is lower than that (80 HV) observed for the quaternary alloy with Mo. The first stage corresponds to the formation of W clusters on the dislocations in the martensitic matrix.

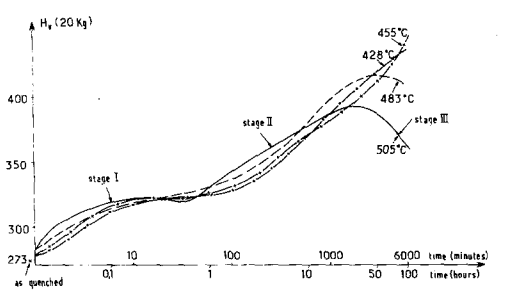

Figure 4 Hardness curves (under hydrogen atmosphere) for the Fe–Ni–Co–W alloy.

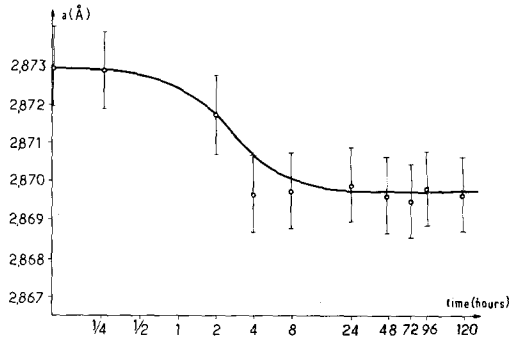

Figure 5 Variation of the martensitic matrix parameter versus time for the Fe–Ni–Co–W alloy aged at 454° C.

Stage II which exhibits a larger increase in the hardness than that observed for stage I, begins at a time which is shorter than the higher ageing temperature; it corresponds to the formation of precipitates that have been studied by electron microscopy (see Section 3.3.)

Stage III which shows a marked decrease in the hardness, corresponds to the formation of the reversed austenite.

In Fig. 5 the lattice parameter of the martensitic matrix is plotted against the ageing time for samples aged at 454° C. The first two stages of the precipitation cannot be distinguished. In fact, during the first fifteen minutes corresponding to the formation of W atom clusters (stage I), no variation in the parameter was observed, while during stage II a clear decrease in the parameter of the martensite occurred.

For stage II only, the kinetics of the precipitation process were determined from resistometric measurements, using the method of calculation which was previously described [23]. For stage I, because of its very short duration, such measurements are not sufficiently precise. The kinetics of isothermal precipitation for stage II fits well the following equation due to Johnson and Mehl [33]:

$$y(t) = 1 - \exp\left[-(kt)^n\right] \qquad (1)$$

where $y(t)$ represents the fraction transformed after a time t, and is equal to

$$\frac{A(0) - A(t)}{A(0) - A(\infty)}$$

where A represents the value of the physical property studied, i.e. the resistivity or the hardness; $A(0)$, $A(t)$ and $A(\infty)$ correspond respectively to times $t = 0$, $t = t$ and $t = \infty$. The coefficient k varies with the temperature and from the theoreti-

TABLE I

Temperature	n	k [h^{-1}]
380	0.52	0.002
426	0.75	0.021
459	0.79	0.069
486	0.91	0.134
525	0.82	0.242

cal models [33], the coefficient n can be related to the nature of the precipitation mechanism.

The difficulty relative to Equation 1 is to determine the value of $A(\infty)$. In fact, during the experiments the value of $A(\infty)$ cannot be easily reached because of the limited duration of the ageing (about 100 h) and the formation of the reversed austenite.

To calculate the parameters k and n a computer program was used to fit the calculated curve to the experimental one. The results obtained from the resistivity measurements are given in Table I.

The values calculated for n as a function of temperature varied between 0.52 and 0.91. For the lower temperatures (i.e. 380° C), n was found to be near 0.66. From the theoretical models of Cottrell and Bilby [34] and Harper [35], this n value may correspond to the precipitation on the dislocations which had been effectively observed in thin foils using electron microscopy. For higher temperatures, n approaches 1. From [33], this value should correspond to the growth of rod-shaped precipitates, controlled by diffusion along the direction of the axis of these rods; such rods were observed by electron microscopy.

The apparent activation energy of the precipitation, Q, was calculated assuming that the rate of the reaction is equal to

$$\frac{dy}{dt} = A \exp\left[-\frac{Q}{RT}\right] \qquad (2)$$

where A is a constant independent of the temperature. For a constant transformed fraction $y(t)$, Equation 2 becomes $\log (t/n) \propto (Q/RT)$.

For various values of the transformed fraction $y(t)$ from 0.05 to 0.95, it was found that Q increases from 107 kJ mol^{-1} to 201 kJ mol^{-1}. For volume diffusion of ^{185}W in b c c iron, the value of the activation energy is 293 kJ mol^{-1} [36]. These results suggest that the growth of the precipitates begins by a pipe diffusion phenomenon. When the ageing time increases, the density of the dislocations in the martensitic matrix decreases and volume diffusion of W atoms occurs.

3.3. Study of stage II by electron microscopy

In the temperature range studied, the formation of a superstructure, or the ω phase, was not observed as it has been in the case of the quaternary alloy with Mo.

For a short ageing time (i.e. a few minutes at 428° C), the dislocations of the martensitic matrix were observed to be slightly decorated, but no extra spots were present on the diffraction patterns of the martensite. For longer ageing times (i.e. 120 h at 408° C, or 17 h and 120 h at 454° C), bright-field micrographs exhibited rod-shaped precipitates of several nm in length. These rods were found to lie in the martensitic matrix in preferential directions. From these precipitates, diffraction patterns were observed identical to those obtained from a maraging steel by Shimizu and Okamoto [22] and attributed to the precipitate Ni_3Mo. The following orientation relationships were determined [22] considering the phase Ni_3Mo of the type $TiCu_3$ [38], with an orthorhombic structure having the parameters $a =$ 0.5064 nm, $b = 0.4224$ nm, $c = 0.4448$ nm [39].

$$(0\,1\,1)_M \parallel (0\,1\,0)_{Ni_3Mo}$$
$$\text{and} \quad [1\,\bar{1}\,1]_M \parallel [1\,0\,0]_{Ni_3Mo} \qquad (3)$$

$$\text{or} \quad (0\,1\,1)_M \parallel (0\,1\,0)_{Ni_3Mo}$$
$$\text{and} \quad [1\,\bar{1}\,1]_M \text{ at } 0.42° \text{ from } [1\,0\,2]_{Ni_3Mo} \qquad (4)$$

Because of the smaller misfit between the interatomic distances along the directions $[1\,\bar{1}\,1]_M$ and $[1\,0\,0]_{Ni_3Mo}$ than along the directions $[1\,\bar{1}\,1]_M$ and $[1\,0\,2]_{Ni_3Mo}$, the relationship including $[1\,\bar{1}\,1]_M \parallel [1\,0\,0]_{Ni_3Mo}$ was adopted.

The diffraction patterns obtained from the (Fe, Ni, Co, W) alloy should therefore be due to the formation and the growth of a precipitate which is isomorphous with Ni_3Mo, i.e. Ni_3W. However, the intermetallic compound Ni_3W had not been found in the binary Ni–W system [37]. The precipitates observed in the quaternary (Fe, Ni, Co, W) alloy might have a more complex composition based on Ni_3W but of the type A_3W where A represents a mixture of Fe, Ni and Co.

In view of the orientation relationship (3), there are twelve variants, and consequently, twelve different families of precipitates should be observed. First, the stereographic projection of the compound A_3W with the pole of the plane (0 1 0) at the centre was constructed using as a first approxi-

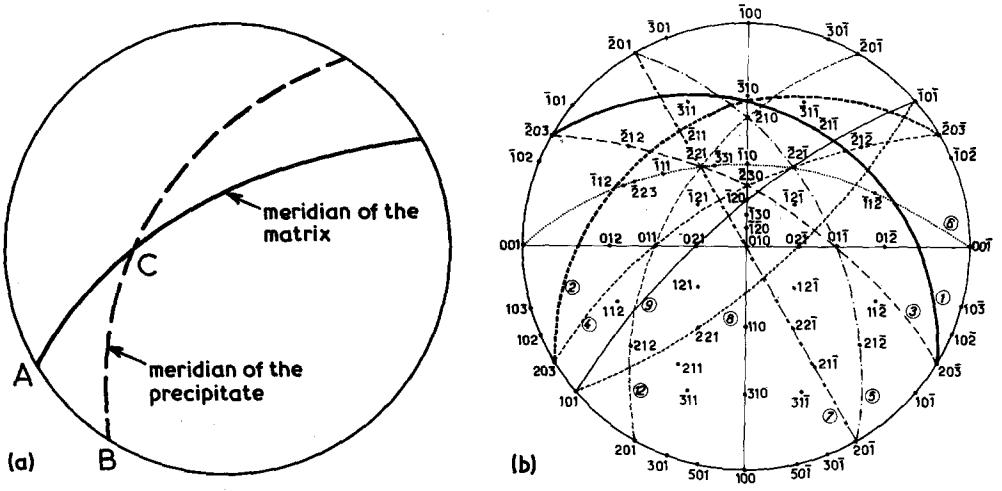

Figure 6 The different meridians corresponding to the different families of precipitates for a martensitic matrix with a zone axis [0 1 3].

mation the values of the parameters of the intermetallic compound Ni_3Mo given above. When the stereographic projections of the martensite and the Ni_3Mo compound were superimposed for a particular variant, it was found that the poles of the planes of the precipitates that were at 90° from a zone axis of the martensitic matrix were not always on the chosen meridian of the matrix, but shifted by a few degrees. Therefore, two meridians must be considered: the meridian of the precipitates and that of the matrix. These two meridians may coincide or may intersect. When they coincide, there is no problem in calculating the theoretical diffraction pattern of the matrix and that of the superimposed precipitates. In fact, the angles between the poles of the matrix plane and the precipitate planes can be easily calculated on the same meridian. When the two meridians intersect at a pole (C in Fig. 6a), which belongs both to the matrix and to the precipitate, the angle made between the pole A of the matrix and the pole B of the precipitate is given by the relation

$$\overrightarrow{AB} = \overrightarrow{AC} - \overrightarrow{BC} \qquad (5)$$

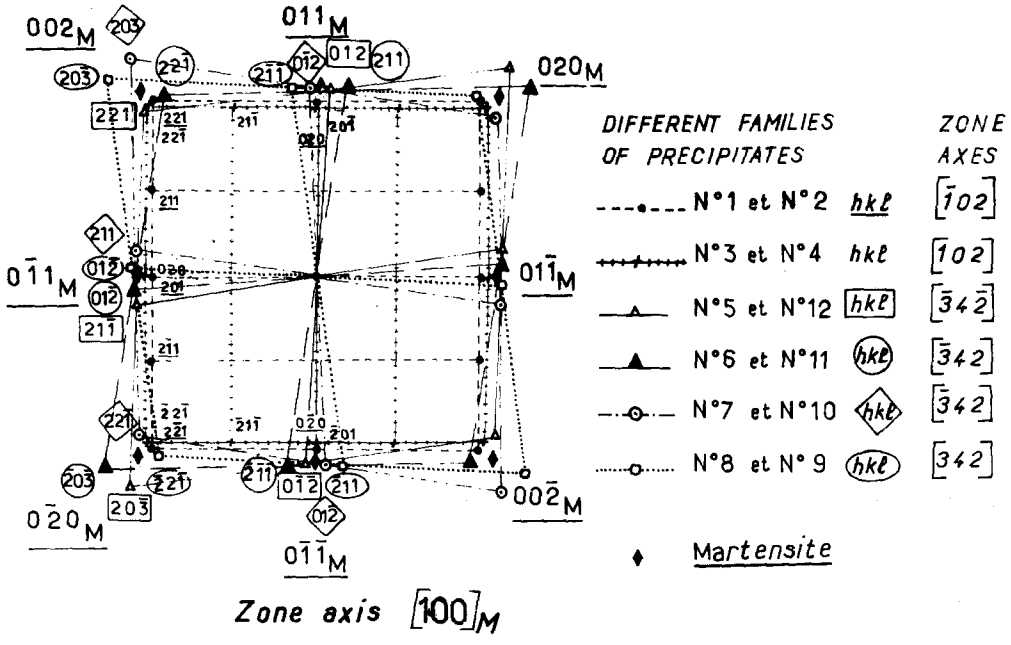

Figure 7 Theoretical diffraction patterns of the precipitates for the zone axis of the martensitic matrix [1 0 0].

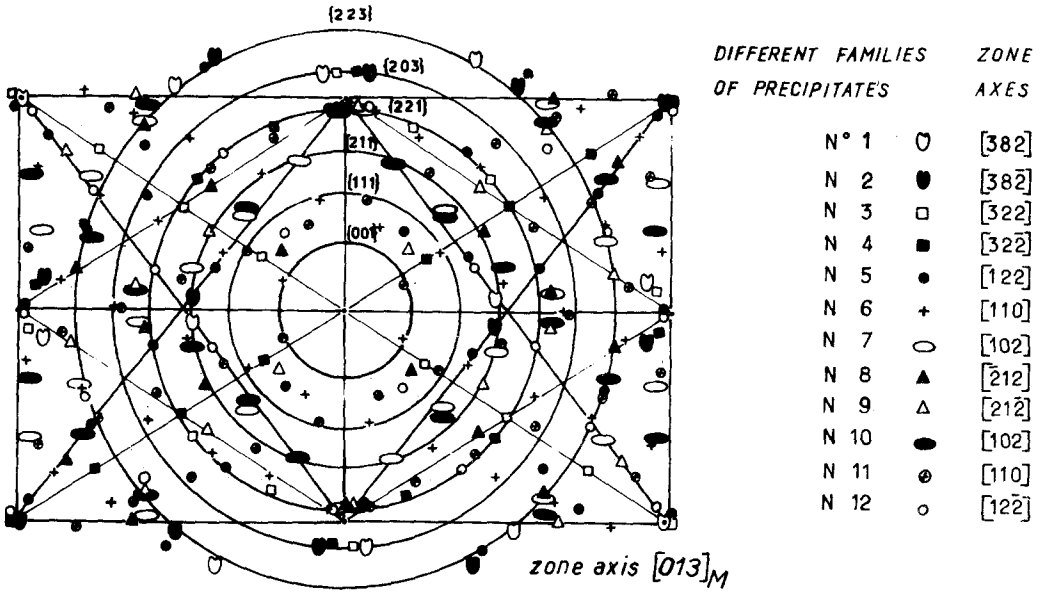

Figure 8 Theoretical diffraction patterns of the precipitates for the zone axis of the martensitic matrix [0 1 3].

The twelve meridians of the precipitates corresponding to the twelve families of the precipitates for the zone axis [0 1 3] of the martensitic matrix are shown in Fig. 6b. The theoretical diffraction patterns for the zone axis [1 0 0] and [0 1 3] of the martensitic matrix are represented in Figs. 7 and 8.

The intensities of the diffracted beams by the $\{h\,k\,l\}$ planes of the supposed intermetallic compound Ni_3W were calculated using the formula

$$I_{e^-\{hkl\}} = \frac{kp|F_{\{hkl\}}|^2}{\sin^2\theta\cos\theta}$$

where θ is the Bragg angle. For electron microscopy, with a wavelength of 0.0037 nm, θ is small, $\cos\theta \simeq 1$, so that

$$I_{e^-\{hkl\}} = kp|F_{\{hkl\}}|^2 d^2$$

where d is the interplanar spacing and p is the multiplying factor.

The atomic scattering factor f can be approximated by the sum of three exponentials

$$f_{e^-}(s) = \Sigma_j A_j \exp[-B_j s^2]$$

where $s = 1/d = 2\sin\theta/\lambda$.

Table II shows the values of A_j and B_j as given in [40]. The relative intensities of the diffracted beams from the $\{h\,k\,l\}$ planes are given in Table III.

TABLE II

Element	A_1	B_1	A_2	B_2	A_3	B_3
Ni	3.382	27.163	2.399	5.216	0.899	0.607
W	5.709	28.782	4.677	5.084	2.019	0.572

TABLE III

Plane $\{h\,k\,l\}$	I/I_0	Plane $\{h\,k\,l\}$	I/I_0	Plane $\{h\,k\,l\}$	I/I_0
0 0 1	5.45	0 1 2	62.91	0 2 2	4.09
1 0 1	11.20	2 1 1	100	2 2 1	15.94
1 1 0	14.72	0 2 1	0.76	0 0 3	0.48
0 1 1	8.59	1 1 2	0.66	3 1 1	0.60
1 1 1	4.56	1 2 1	2.73	1 2 2	1.61
2 0 0	3.34	2 0 2	0.23	1 0 3	0.02
0 0 2	9.16	2 2 0	1.38	0 1 3	0.02
2 0 1	34.97	3 0 1	0.87	1 3 0	0.71
0 2 0	49.05	3 1 0	1.22	1 1 3	1.35
1 0 2	2.66	2 1 2	2.00	3 0 2	0.58

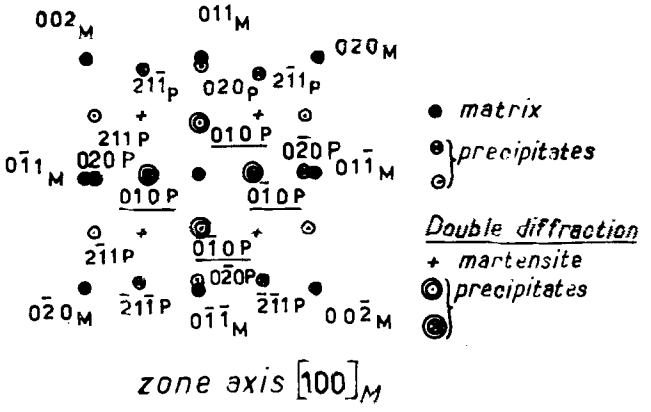

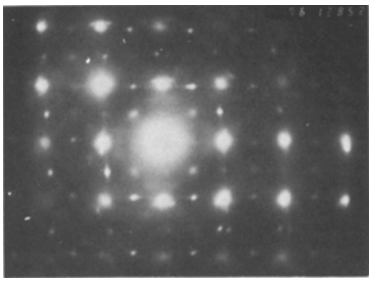

Figure 9 Experimental diffraction patterns obtained on the Fe–Ni–Co–W alloy aged for 120 h at 408° C.

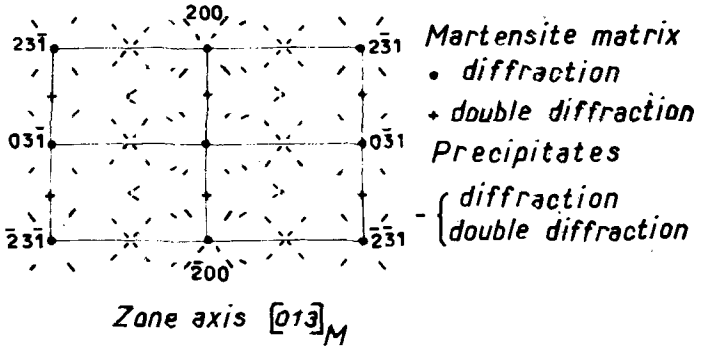

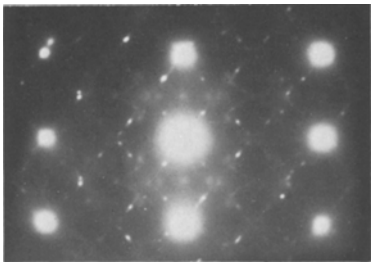

Figure 10 Experimental diffraction patterns obtained on the Fe–Ni–Co–W alloy aged for 120 h at 454° C.

From these results it is seen that the theoretical patterns are in good agreement with those obtained experimentally (Figs. 9 and 10).

In the case of the diffraction pattern with the zone axis [1 0 0], because of the size of the objective aperture and of the proximity of the very intense diffraction spots of the matrix, only four families of the precipitates can be obtained experimentally. These families appear parallel in pairs. Two families are seen in Fig. 11a, the others are seen in Fig. 11b.

The diffraction spots tend to be disc-shaped which correspond well with the observation of rod-shaped precipitates. Furthermore the direc-

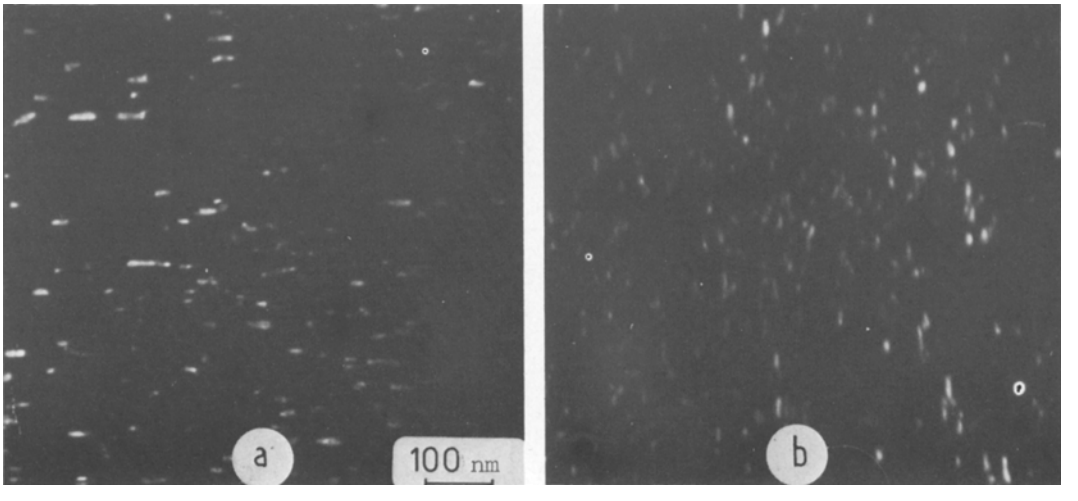

Figure 11 Dark-field micrographs obtained (a) from the spot (2 1 1) (families 1 and 2), (b) from the spot (2 1 $\bar{1}$) (families 3 and 4), on the alloy aged for 120 h at 408° C, zone axis $[1\,0\,0]_M$.

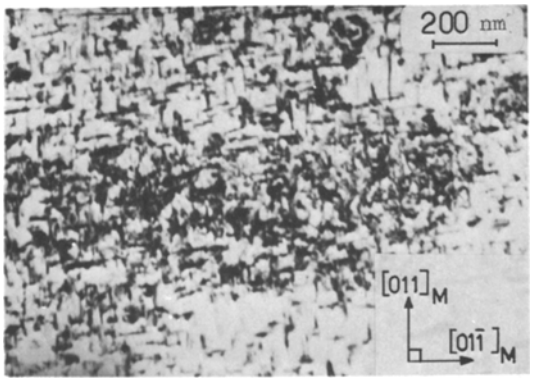

Figure 12 Bright-field micrograph obtained on the Fe–Ni–Co–W alloy aged for 120 h at 454° C, zone axis $[1\,0\,0]_M$.

tion of elongation of the diffraction spots of the precipitates coincide with the $[0\,1\,1]^*$ and $[0\,1\,\bar{1}]^*$ directions of the martensitic matrix (Fig. 9). From these data the indices of the projected directions of the rods in the direct lattice on the plane $(1\,0\,0)$ were calculated to be:

$$[0\,1\,1]^* \times [1\,0\,0]^* = [0\,1\,\bar{1}]$$

and

$$[0\,1\,\bar{1}]^* \times [1\,0\,0]^* = [0\,\bar{1}\,\bar{1}]$$

The angle between $[0\,1\,\bar{1}]$ and $[0\,\bar{1}\,\bar{1}]$ is 90°. This value agrees well with the angle between the mean direction of elongation of the four families of the precipitates observed in bright- and dark-field micrographs (Figs. 11ab and 12). As expected, the same average size for the four different families of precipitates on the dark-field micrographs was observed.

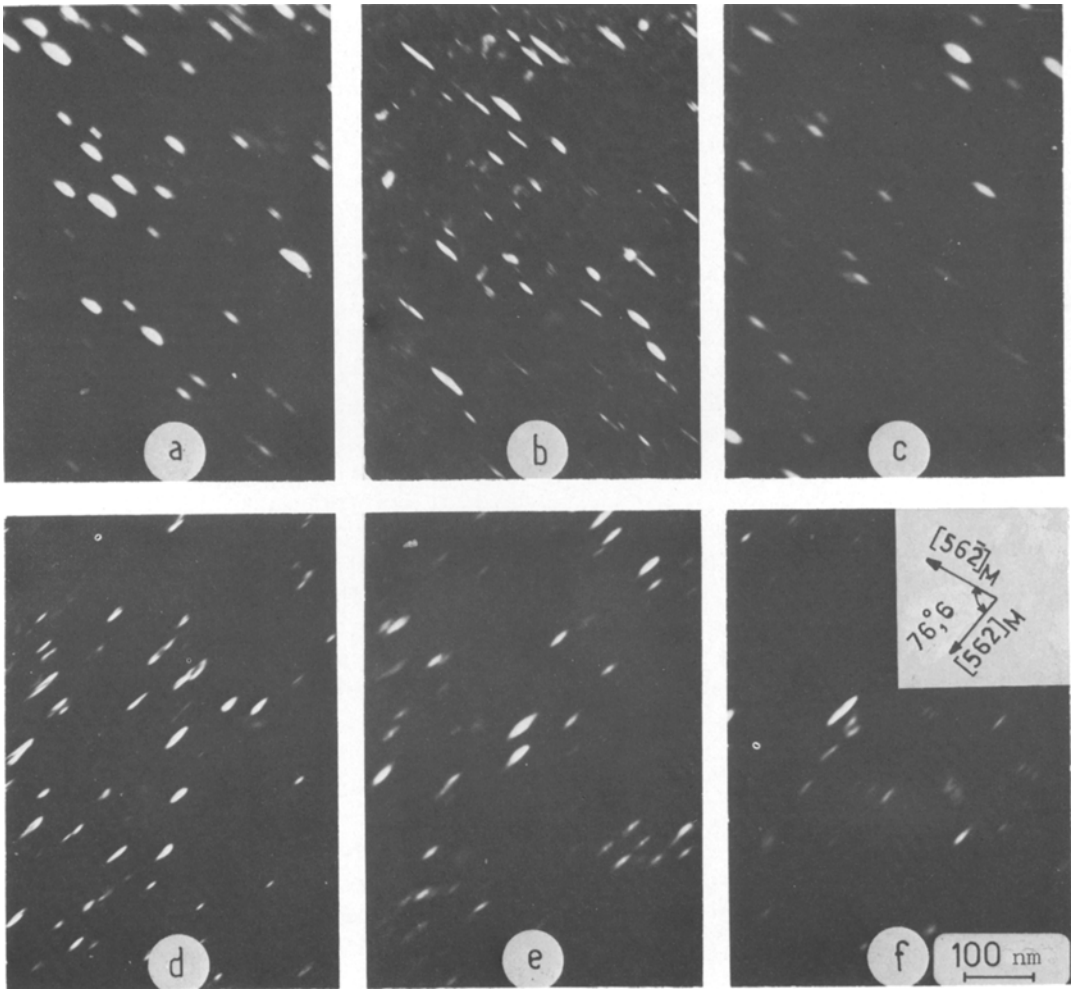

Figure 13 Dark-field micrographs obtained on the Fe–Ni–Co–W alloy aged during 120 h at 454° C, showing six different families of rod precipitates making an angle of $\simeq 80°$ between them, zone axis $[0\,1\,3]_M$.

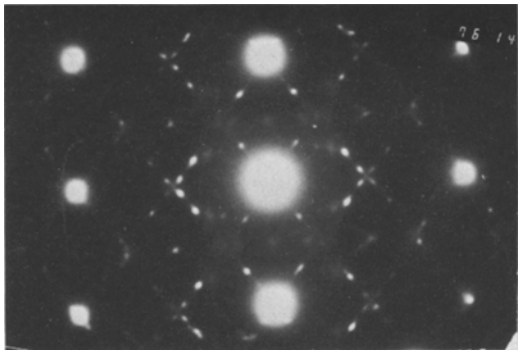

Figure 14 Diffraction pattern obtained on the alloy 65 wt% Fe–17 wt% Ni–8 wt% Co–10 wt% W aged during 120 h at 454° C, zone axis $[0\,1\,3]_M$.

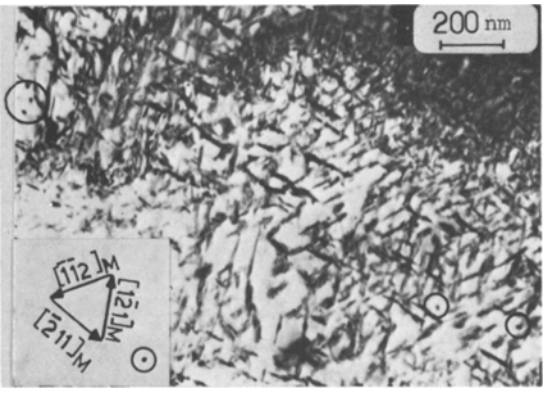

Figure 15 Bright-field micrographs obtained on the Fe–Ni–Co–W alloy aged during 120 h at 454° C, zone axis $\langle 1\,1\,1\rangle_M$.

In the case of the diffraction pattern, with the zone axis [0 1 3] of the martensite, it is possible in principle to observe all twelve families of precipitates in the corresponding dark-field micrographs. For an ageing time of 120 h at 454° C, six families corresponding to numbers 1, 2, 5, 12, 7 and 10 respectively were readily observed, (Fig. 13). The remaining six families presumably gave images too faint to see. To reveal all twelve families, the volume fraction of precipitate was increased by using a higher W content (65 Fe–17 Ni–8 Co–10 W alloy). In the event, only eight families were visible; in fact, on the diffraction pattern obtained from this alloy aged during 120 h at 454° C (Fig. 14), it is easier to reveal the families designated as numbers 3 and 4 but it is always difficult to reveal the families marked 6, 8, 9 and 11 on the theoretical diffraction pattern. These latter give rise to very faint diffraction spots.

In the diffraction pattern shown in Figs. 9 or 14, the diffraction spots of the different families of precipitates, designated as 1, 2, 5, 12, 7 and 10, are elongated along the directions $[\bar{4}\,3\,\bar{1}]^*$ and $[4\,3\,\bar{1}]^*$ of the martensitic matrix. In the direct lattice, the indices of the projected directions of the rods are given respectively by

$$[\bar{4}\,3\,\bar{1}]^* \times [0\,1\,3]^* = [5\,6\,\bar{2}]$$

$$[4\,3\,\bar{1}]^* \times [0\,1\,3]^* = [5\,\bar{6}\,2]$$

These two directions make an angle of 76.65°. From the dark-fields, the average value of the angle between the rods is about 80°. For the other six families of precipitates, the elongations of the diffraction spots are along the directions $[2\,3\,\bar{1}]^*$ and $[\bar{2}\,3\,\bar{1}]^*$ of the martensitic matrix (Fig. 14). In the direct lattice, the indices of the projected directions of the rods are respectively $[5\,\bar{3}\,1]$ and $[5\,3\,\bar{1}]$. These projections make an angle of 64.62° but because of the very faint spots given by these families, this value could not be verified.

From the indices of the projections of the preferential directions of growth of the precipitates, it is easy to determine the indices of these directions of the direct lattice of the martensitic matrix, i.e. $\langle 1\,1\,1\rangle$. It has been verified on a bright-field, corresponding to a zone axis $\langle 1\,1\,1\rangle$ that the different families of precipitates are elongated along the three directions $[1\,\bar{2}\,1]$, $[\bar{2}\,1\,1]$, $[\bar{1}\,\bar{1}\,2]$, making a mutual angle of 60° (Fig. 15). The fourth direction $\langle 1\,1\,1\rangle$ cuts the bright-field perpendicularly and the precipitates appear as points surrounded by circles in Fig. 15.

Thus, from the experimental diffraction patterns, the preferential direction of growth of the precipitates is confirmed to be $\langle 1\,1\,1\rangle$, identical to that found by Shimizu and Okamoto [22] for the Ni_3Mo precipitates in a maraging steel.

The present results agree well with the Ni_3W formula proposed by Yedneral *et al.* [32] for the precipitates formed in very W enriched alloys, except that no large precipitates of pure W have been found during ageing at 454° C, of the alloy containing only 4.87 wt% W. From the diffraction patterns, the values of the parameters of the A_3W precipitates have been determined. For this purpose, the electron microscope length constant was calibrated by making use of the lattice parameter of the martensite, which had been separately calibrated by X-rays. The parameters calculated for $(Fe, Ni, Co)_3W$ are

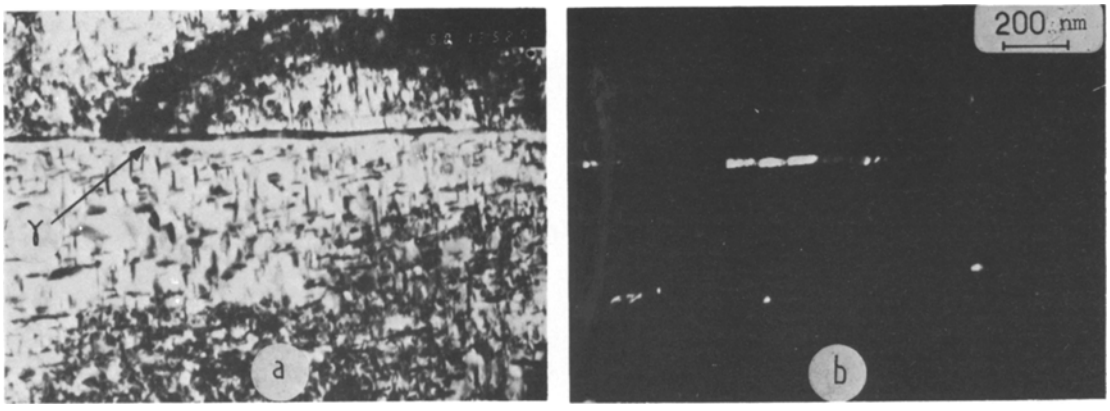

Figure 16 (a) and (b) Bright- and dark-field micrographs of the same areas showing the formation of reversed austenite, zone axis $[1\,0\,0]_M$.

$$a = (0.508 \pm 0.01)\,\text{nm}$$

$$b = (0.415 \pm 0.01)\,\text{nm}$$

$$c = (0.425 \pm 0.01)\,\text{nm}$$

When these values are compared with those of the compound Ni_3Mo equal to $a = 0.5064$ nm, $b = 0.4224$ nm and $c = 0.4448$ nm, it was concluded that as a first approximation the stereographic projection of Ni_3Mo could be used to construct the theoretical diffraction patterns of the A_3W precipitate.

In the case of the ageing carried out at 454° C during 120 h, the formation of a small amount of reversed austenite was observed especially along the boundaries of the laths of the martensite, Figs. 16a and b.

4. Conclusions

It has been shown that during a simple thermal cycle (between 20° C and 950° C) at a moderate rate (300° Ch^{-1}), the behaviour of the two alloys Fe–18.65 wt %Ni–8.99 wt %Co–4.87 wt %W and Fe–18.65 wt %Ni–8.99 wt %Co–4.87 wt %Mo is similar. In fact, below the A_{s_0} point, the martensite decomposes into two phases, the former enriched with W or Mo, the latter depleted in the same elements.

During isothermal ageing, in the case of the alloy with Mo, Mo-rich clusters form first, then ω phase. In the case of the alloy with W, the ω phase has not been observed, but an intermetallic precipitate isomorphous with Ni_3Mo was found of composition A_3W (where A represents Fe, Ni and Co together). The precipitates are rod-shaped, of several nm in length. This fact is consistent with the fact that the n Johnson–Mehl parameter was found to be approximately equal to unity. The preferred direction of growth of these precipitates is $\langle 1\,1\,1 \rangle$ in the martensitic matrix and the orientation relationship with the martensitic matrix is

$$(0\,1\,1)_M \parallel (0\,1\,0)_{A_3W}$$

and

$$[1\,\bar{1}\,1]_M \parallel [1\,0\,0]_{A_3W}$$

identical to that found for the Ni_3Mo precipitate in the (Fe, Ni, Co, Mo) maraging alloy.

Among the twelve theoretical families of precipitates, eight have been easily observed.

The parameters of A_3W are very close those of Ni_3Mo.

Prior to the formation of the A_3W precipitates, the dislocations of the martensitic matrix were observed to be slightly decorated.

References

1. "Les aciers Maraging à 18% de Ni au Co, Mo", Revue du Nickel, **28** (1962).
2. S. FLOREEN and R. F. DECKER, *Trans. Quart. ASM* **55** (1962) 518.
3. J. PITAUD, "Les aciers Maraging", Extrait de la Revue du Nickel, **29** (1963).
4. B. G. REISDORF, *Trans. ASM* **56** (1963) 783.
5. G. P. SPEICH, *Trans. Met. Soc. AIME* **227** (1963) 1426.
6. S. FLOREEN, *Trans. Quart. ASM* **57** (1964) 38.
7. A. J. BAKER and P. R. SWANN, *Trans. ASM* **57** (1964) 1008.
8. R. K. PITLER and G. S. ANSELL, *Trans. ASM* **57** (1964) 220.
9. G. P. MILLER and W. I. MITCHELL, *J. Iron Steel Inst.* **203** (1965) 899.
10. H. MARCUS, L. H. SCHWARTZ and M. E. FINE, *Trans. ASM* **59** (1966) 468.
11. R. B. BANERJEE, J. M. CAPENOS and J. J.

HAUSER, "Advances in electron metallography" 6 *ASTM STP* 396 (American Society for Testing Metals, Metals Park, Ohio, 1966) p. 115.
12. D. T. PETERS and C. R. CUPP, *Trans. Metal. Soc. AIME* **236** (1966) 1420.
13. K. DETERT, *Arch. Eisenhüttenwesen* **37** (1966) 579.
14. J. R. MIHALISIN, *Trans. ASM* **59** (1966) 60.
15. R. D. GARWOOD and R. D. JONES, *J. Iron Steel Inst.* **204** (1966) 512.
16. M. J. FLEETWOOD, G. M. HIGGINS and G. P. MILLER, *J. Appl. Phys.* **16** (1965) 645.
17. J. M. CHILTON and C. J. BARTON, *Trans ASM* **60** (1967) 528.
18. W. R. BANDI, J. L. INTZ and L. M. MELNICK, *J. Iron Steel Inst.* **207** (1969) 348.
19. C. SERVANT and G. CIZERON, *Mém. Sci. Rev. Mét.* **LXVI** (1969) 531.
20. C. SERVANT, G. MAEDER, G. CIZERON and P. LACOMBE, *Mém. Sci. Rev. Mét.* **LXVIII** (1971) 201–213.
21. J. BOURGEOT, P. MAITREPIERRE, J. MANENC and B. THOMAS, Fifth International Symposium, University of California, Berkeley, California (1971).
22. KEN'ICHI SHIMIZU and HISAKI OKAMOTO, *Trans. Japan Inst. Metals* **12** (1971) 273.
23. C. SERVANT, Thèse de Doctorat ès-Sciences Université Paris-Sud, Orsay (1972).
24. A. F. YEDNERAL and M. D. PERKAS, *Fiz. metal. metalloved* **33** (1972) 315.
25. R. COURRIER, Thèse de Doctorat ès-Sciences, Université de Nancy (1972).
26. R. COURRIER and G. LE CAER, *Mém. Sci. Rev. Mét.* **LXXI** (1974) 692.
27. C. SERVANT, G. MAEDER and G. CIZERON, *Met. Trans.* **6A** (1975) 981.
28. G. MAEDER, Thèse de Doctorat ès-Sciences, Université de Paris-Sud, Orsay (1975).
29. A. AGNEL, F. HEDIN, G. MAEDER, C. SERVANT and P. LACOMBE, *Acta Met.* **25** (1977) 1445.
30. C. SERVANT and P. LACOMBE, *J. Mater. Sci.* **12** (1977) 1807.
31. C. SERVANT, G. MAEDER and P. LACOMBE, *Met. Trans.* (to be published).
32. A. F. YEDNERAL, O. P. ZHUKOV and M. D. PERKAS, *Fiz. Met. Metalloved* **36** (1973) 339 and; 569.
33. J. BURKE, "La cinétique des changements de phase dans les métaux", (Masson, Paris, 1968).
34. A. H. COTTRELL and B. A. BILBY, *Proc. Phys. Soc.* **A62** (1949) 49.
35. S. HARPER, *Phys. Rev.* **83** (1951) 209.
36. P. L. GRUZIN, *Dokl. Akad. Nauk.* **94** (1954) 81.
37. M. HANSEN, "Constitution of Binary Alloys" (McGraw-Hill, New York, 1958) p. 1057.
38. N. KARLSON, *J. Inst. Metals.* **79** (1951) 391.
39. SHOZO SAITO and P. A. BECK, *Trans. AIME* **215** (1959) 938.
40. G. H. SMITH and R. E. BURGE, *Acta Cryst.* **15** (1962) 182.

Received 6 June and accepted 3 October 1979.